Identifying the order-parameter symmetry of superconducting $PrOs_4Sb_{12}$ by Andreev reflection spectroscopy: Evidence for unconventional pairing involving multiple bands

S. H. Curnoe[1], C. S. Turel[2], S. Bohloul[1,3], W. M. Yuhasz[4], R. Baumbach[4], M. B. Maple[4] and J. Y. T. Wei[1,5]
[1]*Department of Physics and Physical Oceanography, Memorial University of Newfoundland, St. John's, NL, A1B 3X7*
[2]*Department of Physics, University of Toronto, 60 St. George Street, Toronto, ON M5S 1A7, Canada*
[3]*Centre for the Physics of Materials and Department of Physics, McGill University, Montreal, PQ, H3A 2T8*
[4]*Department of Physics and Center for Advanced Nanoscience, University of California San Diego, La Jolla, California 92093 and*
[5]*Canadian Institute for Advanced Research, Toronto, ON, M5G1Z8 Canada*

Point-contact Andreev reflection spectroscopy was performed on single crystals of the heavy-fermion superconductor $PrOs_4Sb_{12}$, down to 90 mK in temperature and up to 3 T in magnetic field. The conductance spectra show multiple structures, including zero-bias peaks and spectral dips, and are interpreted as evidence for unconventional pairing involving two different bands. Samples with 2% Ru replacing Os were also measured, showing the emergence of a pronounced spectral hump. The results of a comprehensive set of spectral calculations using the Blonder-Tinkham-Klapwijk theory of Andreev reflection are presented. All symmetry-allowed gap functions are considered, including several non-unitary cases. Several candidate gap functions are identified that reproduce the main features of our experimental data; among these, the superconducting phase with symmetry $C_3 \times \mathcal{K}$ agrees best with other previous measurements.

PACS numbers: 74.70.Tx, 74.45.+c, 74.25.Dw, 74.20.Rp

I. INTRODUCTION

Superconductivity in heavy-fermion materials has been a heavily researched topic, particularly for the role that strongly-correlated electrons play in the pairing process. The discovery of superconductivity in the filled skutterudite $PrOs_4Sb_{12}$ has attracted much attention, because it is the first heavy-fermion superconductor containing neither Ce nor U, but rather Pr atoms which show no ground-state magnetic order[1]. Various unconventional properties have been reported in the superconducting state of $PrOs_4Sb_{12}$[2]. Of particular interest is the appearance of low-energy quasiparticle excitations[1,5–10], characteristic of a nodal superconducting gap function. Also intriguing is the occurence of a second density-of-states discontinuity just below the superconducting critical temperature (T_c)[3,4], indicative of a second phase transition. Furthermore, angular magneto-thermal conductivity measurements have observed that the pairing symmetry of $PrOs_4Sb_{12}$ undergos a phase transition in a magnetic field[9]. Such a complex order-parameter (OP) phase diagram suggests the presence of either multiple superconducting OPs or a multi-dimensional OP, reminiscent of the case of UPt_3[11].

There have been conflicting experimental reports on the superconducting gap topology of $PrOs_4Sb_{12}$, some indicating the presence of gap nodes while others indicating the Fermi surface to be fully gapped[12]. To reconcile the difference between these reports, a recent proposal has invoked the multi-band dispersion of $PrOs_4Sb_{12}$[13] to suggest that there are two superconducting gaps, i.e. a nodal gap in a light-mass band and a non-nodal gap in a heavy-mass band[14,15]. Double superconducting gaps have been observed in two separate thermal-conductivity measurements[16,17]. However, whereas the earlier measurement indicated both gaps to have s-wave symmetry[16], the more recent measurement indicated only one s-wave gap with the other gap having nodal symmetry[17]. The latter result suggests that there are two distinct OPs with different pairing symmetries and T_c's in $PrOs_4Sb_{12}$. Although still under debate, this multi-band and multi-symmetry scenario could also explain the two T_c's seen in heat-capacity measurements on $Pr(Os_{1-x}Ru_x)_4Sb_{12}$, where the nodal gap becomes dominated by a non-nodal gap for Ru-doping above $\approx 1\%$[7].

Despite these prior studies, the symmetry of the superconducting OP in $PrOs_4Sb_{12}$ is still not known. In this paper, we report on point-contact Andreev reflection spectroscopy (PCARS) measurements of $PrOs_4Sb_{12}$ single crystals, and identify the OP symmetry by analyzing the data with first-principle spectral simulations. PCARS is an inherently local and phase-sensitive probe of the superconducting OP[20], and has been used to study the pairing state of several unconventional superconductors, including cuprates[21], ruthenates[22,23], borocarbides[24], MgB_2[25] and heavy-fermion metals[26,27]. Our PCARS measurements on $PrOs_4Sb_{12}$ show conductance spectra with multiple features, including zero-bias peaks and spectral dips, which are interpreted as evidence of unconventional pairing. The spectral evolution down to 90 mK in temperature and up to 3 T in field reveal a phase diagram characteristic of multiband pairing. Samples with 2% Ru replacing Os were also measured, showing the emergence of a pronounced spectral hump. To relate the data to the superconducting OP symmetry, we performed spectral simulations based on all possible OP phases allowed by the crystal symmetry of $PrOs_4Sb_{12}$. Our spectral analysis indicates that a sin-

gle superconducting phase of the T_g OP, present on two different bands, can account for the data. We discuss the most likely of possible OP phases by comparing our results with other experimental results on $PrOs_4Sb_{12}$.

II. EXPERIMENTAL RESULTS

The single crystals used in our experiment were grown with a molten metal-flux method[28]. For the undoped $PrOs_4Sb_{12}$ crystals, electrical resistivity measurements showed a single T_c at $\approx$ 1.85 K with $\approx$ 5 mK transition width, and an upper critical field $H_{c2} \approx 2.25$ T at 200 mK. AC susceptibility $\chi(T)$ showed two T_c's, $T_{c1} \approx 1.85$ K and $T_{c2} \approx 1.65$ K, similar to previously reported results[3,29]. PCARS measurements were performed in a ^{3}He-^{4}He dilution refrigerator, using Pt-Ir tips on c-axis faces of the crystals. Prior to measurement, the crystals were etched in a 1:1 HNO_3-HCl mixture to remove any residual Sb flux. Junction impedances were typically 0.5-1 Ω, resulting in point contacts which were in the ballistic regime[30]. To minimize Joule heating, a pulsed-signal four-point technique[31] was used to acquire current-*vs.*-voltage I-V curves, which were numerically differentiated to yield dI/dV spectra.

Fig. 1(a) shows the temperature evolution of dI/dV spectra of $PrOs_4Sb_{12}$ in zero magnetic field. At 90 mK, well below $T_{c1} \approx 1.85$ K, there is a pronounced zero-bias peak (ZBP) accompanied by a symmetric dip which begins at $\approx \pm 0.4$ mV, as indicated by δ_1 in the figure. An additional dip is also present at $\approx \pm 0.2$ mV, as indicated by δ_2. With increasing temperature, the ZBP decreases in height and the dips move inward. The spectrum flattens out above $T_{c1} \approx 1.85$ K, consistent with the sample no longer being superconducting.

Fig. 1(b) shows the detailed temperature evolution of the ZBP height and of the positions δ_1 and δ_2, after normalizing them relative to their maximum values. Also plotted in Fig.1(b) is the excess spectral area, which is defined by subtracting each dI/dV spectrum by the normal-state spectrum and then numerically integrating between ± 1.8 mV. These plots indicate that the evolution of the various spectral features is governed by two distinct temperature scales, corresponding respectively to $T_{c1} \approx 1.85$K and $T_{c2} \approx 1.65$K.

Figure 2(a) shows the magnetic-field evolution of dI/dV spectra measured at 90 mK. As the field is increased, the ZBP decreases in height and the dip structures move inward, qualitatively similar to the spectral evolution with temperature. However, the ZBP height collapses more quickly with field than with temperature, relative to the evolution of the excess spectral area. As shown in Figure 2(b), the ZBP height vanishes above ≈ 1.5 T while the excess area persists up to ≈ 2.3 T. This field evolution indicates that there are also two different energy scales governing the field suppression of superconductivity in $PrOs_4Sb_{12}$. Namely, the low-Z Andreev states are spectrally robust up to a lower-field boundary $H' \approx 1.5$ T at 90 mK, while the high-Z Andreev states persist up to a higher-field boundary $H'' \approx 2.3$ T at 90 mK. It is worth noting that PCARS data taken on UPt_3[38], which is known to have multi-component superconducting OP[11], also shows spectral features that vanish at a field boundary lower than H_{c2}.

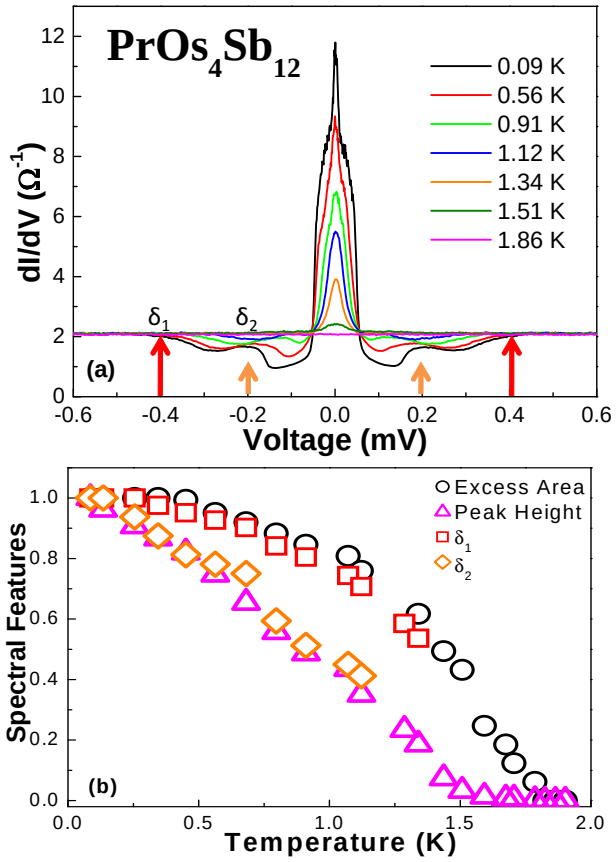

FIG. 1: (color online). (a) Differential conductance as a function of temperature for a Pt-Ir/$PrOs_4Sb_{12}$ point-contact junction in zero magnetic field. (b) Temperature dependence of various spectral features, after normalizing relative to their maximum values. The triangles correspond to zero-bias peak height, the squares and diamonds to δ_1 and δ_2. The circles correspond to the excess spectral area, as defined in the text.

To map out a detailed H-T phase diagram for $PrOs_4Sb_{12}$, we carried out a combined analysis of the temperature and field evolutions of our data. Figure 3 shows a master plot of the full temperature dependencies of H' and H'' determined from our spectroscopy data, along with $H_{c2}(T)$ determined from our $\rho(T,H)$ data. First, it is clear that $H''(T)$ coincides with $H_{c2}(T)$, indicating that the higher-field boundary is just the resistive upper-critical field. Second, $H''(T)$ and $H'(T)$ appear to emerge from different low-temperature asymptotes and gradually approach each other with increasing temperature. This *non-parallel* behavior between $H''(T)$ and $H'(T)$ resembles the H-T phase diagram determined from angular magneto-thermal conductivity in Ref.[9], in contrast to *parallel* phase boundaries determined from

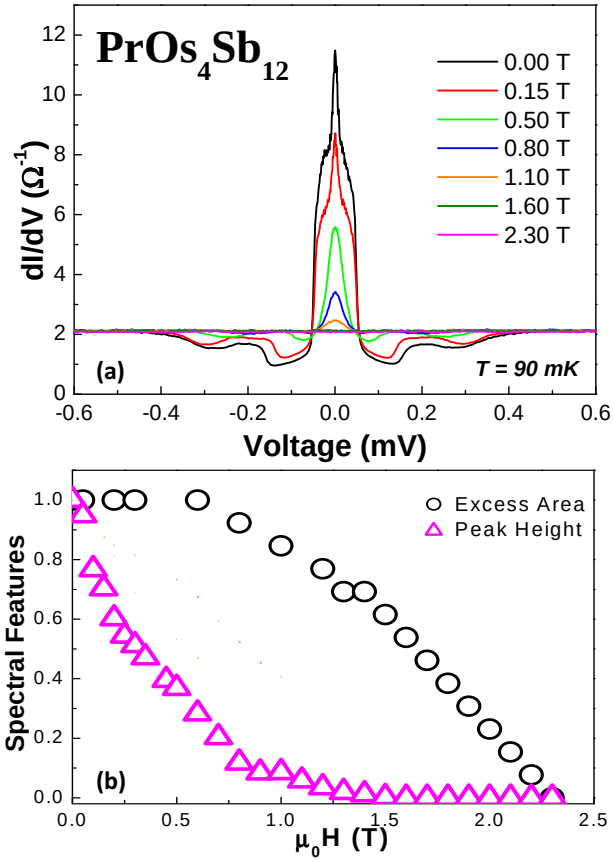

FIG. 2: (color online). (a) Differential conductance as a function of magnetic field for a Pt-Ir/$PrOs_4Sb_{12}$ point-contact junction at 90mK. (b) Field dependence of the zero-bias peak height and excess spectral area, as defined in the text.

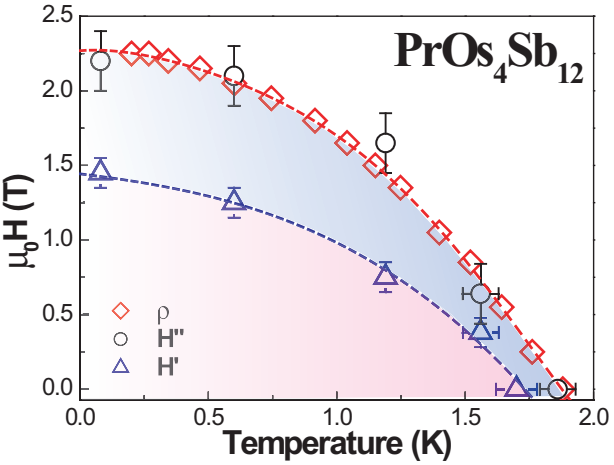

FIG. 3: (color online). Magnetic field vs. temperature phase diagram determined from our point-contact spectroscopy and resistivity data on $PrOs_4Sb_{12}$. H' (triangles) correspond to the field at which the ZBP vanishes. H'' (circles) correspond to the field at which the excess spectral area vanishes. H_{c2} (diamonds) is the upper-critical field measured by resistivity. Dotted curves are added to guide the eye.

heat capacity in Ref.[39]. Finally, our $H''(T)$ and $H'(T)$ curves appear to approach zero at different temperatures, $\approx$ 1.85 K and $\approx$ 1.65 K respectively, agreeing well with T_{c1} and T_{c2} measured by $\chi(T)$ on our samples. *Here it is important to emphasize that our H-T diagram is determined spectroscopically with a highly local probe, thus arguing strongly against sample inhomogeneity as the cause of multiple T_c's.* It should also be noted that although our H-T diagram is qualitatively similar with the one reported in Ref.[9], there is a large quantitative difference in the low-temperature asymptote between our $H'(T)$ and their lower-field boundary $H^*(T)$. Interestingly, surface impedance measurements on $PrOs_4Sb_{12}$ have also indicated a lower-field phase boundary with a zero-temperature asymptote of $\approx$ 1.5 T[40], which is quantitatively consistent with our $H'(T)$.

To probe the effects of Ru-doping, we also measured $Pr(Os_{0.98}Ru_{0.02})_4Sb_{12}$ crystals. These 2% Ru-doped crystals have $T_c \approx 1.8$ K and $H_{c2} \approx 2.2$ T at 200 mK. Figure 4(a) plots the temperature evolution of a typical dI/dV spectrum. At 90 mK, a ZBP is also observed, but its height is lower than in the undoped case. Broad hump structures clearly emerge at $\approx \pm 1.4$ mV and $\approx \pm 0.6$ mV as indicated by δ_3 and δ_4, respectively, in the figure. With increasing temperature, the ZBP decreases in height while the humps become narrower, and the spectrum completely flattens out above $T_c \approx 1.8$ K. The inset of Fig. 4(a) shows the spectral evolution with magnetic field at 90 mK. While the ZBP collapses into the hump structures above $\approx$ 1.5 T, a spectral hump is still visible up to $\approx$ 2.2 T, unlike the undoped case which shows no pronounced humps (Fig. 2(a)). Figure 4(b) plots the temperature dependences of the ZBP height, the excess spectral area, and the positions of δ_3 and δ_4, using the same data reduction as for Fig. 1(b). Comparing Fig. 4(b) and Fig. 1(b), it is clear that while both cases show excess spectral area up to the resistive T_c, Fig. 4(b) shows a more rapid ZBP collapse with temperature. These observations indicate the emergence of a non-nodal gap function with Ru-doping, in agreement with both heat-capacity and penetration-depth measurements[7,41]. Further measurements of crystals with higher Ru-doping levels are under way to elucidate this possibility.

III. THEORETICAL MODELING OF CONDUCTANCE SPECTRA

A. Possible types of superconducting order parameters for $PrOs_4Sb_{12}$

$PrOs_4Sb_{12}$ crystallises in the space group $Im\bar{3}$ with point group T_h. The classification of superconducting order parameters (OP's) was described in Refs.[42,43] for the point groups O_h, D_{6h} and D_{4h} and extended to the point group T_h in Ref.[44]. Here we summarise these re-

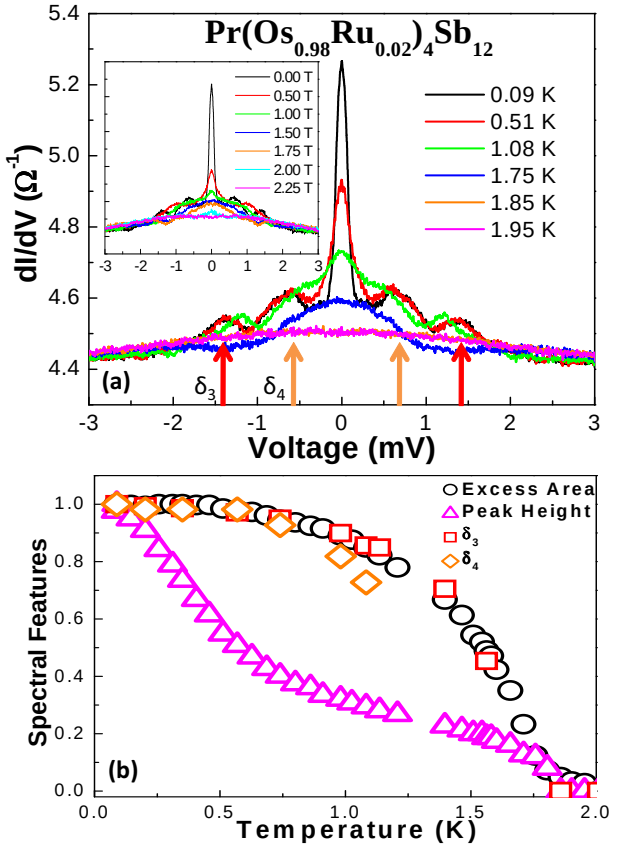

FIG. 4: (color online). (a) Differential conductance spectrum as a function of temperature for a Pt-Ir/$Pr(Os_{0.98}Ru_{0.02})_4Sb_{12}$ point-contact junction in zero magnetic field. The inset shows the spectral evolution versus field at 90 mK. (b) Temperature dependence of the ZBP height and excess spectral area, defined in the same way as in Fig. 1.

sults.

The point group T_h has one one-dimensional OP ($A_{g,u}$), one two-dimensional OP ($E_{g,u}$) and one three-dimensional OP ($T_{g,u}$) in each of the singlet (subscript g) and triplet (subscript u) channels. The A_g OP is "conventional", while the rest are "unconventional". The appearance of an A_g OP is accompanied by no symmetry breaking apart from gauge symmetry. The other OP's always involve a lowering of the point group symmetry. s-wave superconductivity (with gap function $\Delta(\vec{k}) = \Delta_0$) belongs to the A_g OP. The A_g OP has no symmetry-required nodes, although "accidental" nodes may be present. Because they are one-dimensional, the $A_{g,u}$ OP's have only one phase associated with them.

The 2D and 3D OP's have potentially more complicated phase diagrams. A catalog of possible phases is given in Ref.[44]; here we focus phases that are directly accessible from the normal state via a second order phase transition. The best way to unambiguously label the various phases is by their point group symmetry. Table I lists possible SC phases along with representative gap functions (to lowest order in $\vec{k}$) for singlet and triplet cases. $\mathcal{K}$ stands for time reversal; symmetry groups that do not possess the element $\mathcal{K}$ have broken time reversal symmetry. Some of the symmetry groups (for example, $T(D_2)$) have elements which are combinations of rotations and phases and/or time reversal. The details of these groups may be found in Ref.[44].

The superconducting gap function is a 2×2 matrix. For singlet pairing it takes the form

$$\Delta(\vec{k}) = \begin{pmatrix} 0 & \psi(\vec{k}) \\ -\psi(\vec{k}) & 0 \end{pmatrix} \quad (1)$$

where $\psi(\vec{k}) = \psi(-\vec{k})$. For triplet pairing, the gap function is

$$\Delta(\vec{k}) = \begin{pmatrix} -d_x(\vec{k}) + id_y(\vec{k}) & d_z(\vec{k}) \\ d_z(\vec{k}) & d_x(\vec{k}) + id_y(\vec{k}) \end{pmatrix} \quad (2)$$

where $\vec{d}(\vec{k}) = -\vec{d}(-\vec{k})$.

The magnitudes of the gaps are given by $\frac{1}{2}\mathrm{Tr}\Delta\Delta^\dagger(\vec{k}) = |\psi(\vec{k})|$ and $[|\vec{d}(\vec{k})|^2 \pm |\vec{q}(\vec{k})|]^{1/2}$ for the singlet and triplet cases respectively. In *non-unitary superconductivity*, $\vec{q}(\vec{k}) = \vec{d}(\vec{k}) \times \vec{d}^*(\vec{k}) \neq 0$, and the gap is double-valued. The phases $T(D_2)$, $C_3(E)$ and $D_2(E)$ in the triplet channel are non-unitary.

Table I also lists for each phase possible secondary OP's. A secondary OP is one whose symmetry is a supergroup of the primary OP. Secondary OP's will appear alongside primary OP's with the same T_c but with a weaker temperature dependence. It is also worth noting that among the phases listed in Table I, $D_2(E)$ is accessible from $D_2(C_2) \times \mathcal{K}$ via a second order phase transition.

We calculated the conductance spectrum for *all* of the trial gap functions listed in Table I, in search of those that yield ZBP's as observed in our PCTS results.

B. BTK theory

We modeled the conductance spectra using the theory invented by Blonder, Tinkham and Klapwijk[35], generalised to include non-unitary superconducting order parameters. According to our set-up of this model, an electron is injected into the superconductor from the $-\hat{z}$ direction with momentum $\vec{k}_1 = (k_{1x}, k_{1y}, k_{1z})$ ($k_{1z} > 0$) and spin s. The normal-superconducting interface is modeled as a δ-function potential of height H at $z = 0$. At the interface, the electron may be reflected as a hole (Andreev reflection) with momentum $-\vec{k}_1$, or it may be reflected as an electron, with momentum $-\vec{k}'_1 = (k_{1x}, k_{1y}, -k_{1z})$. It may also be transmitted into the superconductor as an "electron-like" quasi-particle, with momentum $\vec{k}_2 = (k_{2x}, k_{2y}, k_{2z})$ ($k_{2z} > 0$) or as a "hole-like" quasi-particle with momentum $\vec{k}'_2 = (-k_{2x}, -k_{2y}, k_{2z})$. In singlet superconductors, the spin of reflected electrons is the same as the incident electron,

TABLE I: Possible superconducting phases for a crystal with tetrahedral (T_h) point group symmetry. The first column lists the OP's, the second column lists the symmetries of the various possible phases, the third and fourth columns give explicit forms for the gap function in the singlet and triplet cases, and the last column lists secondary order parameters. $\varepsilon = e^{i2\pi/3}$, and a, b, η_1 and η_2 are arbitrary real numbers.

OP	symmetry	gap function singlet $\psi(\vec{k})$	gap function triplet $\vec{d}(\vec{k})$	secondary SC OP's
A	$T \times \mathcal{K}$	$k_x^2 + k_y^2 + k_z^2$	(k_x, k_y, k_z)	none
E	$T(D_2)$	$k_x^2 + \varepsilon k_y^2 + \varepsilon^2 k_z^2$	$(k_x, \varepsilon k_y, \varepsilon^2 k_z)$	none
E	$D_2 \times \mathcal{K}$	$ak_x^2 + bk_y^2 - (a+b)k_z^2$	$(ak_x, bk_y, -(a+b)k_z)$	A
T	$D_2(C_2) \times \mathcal{K}$	$k_x k_y$	$(bk_y, ak_x, 0)$	none
T	$C_3 \times \mathcal{K}$	$k_y k_z + k_z k_x + k_x k_y$	$(ak_z + bk_y, ak_x + bk_z, ak_y + bk_x)$	A
T	$C_3(E)$	$k_y k_z + \varepsilon k_z k_x + \varepsilon^2 k_x k_y$	$(\varepsilon a k_z + \varepsilon^2 b k_y, \varepsilon^2 a k_x + b k_z, a k_y + \varepsilon b k_x)$	E $(T(D_2))$
T	$D_2(E)$	$\eta_1 k_y k_z + i\eta_2 k_z k_x$	$(\eta_1 b k_y + i\eta_2 a k_z, \eta_1 a k_x, i\eta_2 b k_x)$	T $(D_2(C_2))$

while the reflected holes have opposite spin to the incident electron; however, in triplet superconductors, if an electron with a given spin is injected then the reflected and transmitted particles may have either spin.

Continuity of the wave function at $z = 0$ requires that $k_{1x} = k_{2x}$, $k_{1y} = k_{2y}$ and $k_{1z} \sin\theta_1 = k_{2z} \sin\theta_2$, where $\theta_{1,2}$ are the polar angles on either side of the barrier. We will assume that E_F is constant across the barrier and so $k_{1z} \approx k_{2z}$. The wavefunction is a four component spinor, which takes the form on the normal side

$$\Psi_{N\uparrow}(\vec{r}) = e^{i\vec{k}\cdot\vec{r}} \begin{pmatrix} 1 \\ 0 \\ a_{\uparrow\uparrow} \\ a_{\uparrow\downarrow} \end{pmatrix} + e^{-i\vec{k}'\cdot\vec{r}} \begin{pmatrix} b_{\uparrow\uparrow} \\ b_{\uparrow\downarrow} \\ 0 \\ 0 \end{pmatrix} \quad (3)$$

$$\Psi_{N\downarrow}(\vec{r}) = e^{i\vec{k}\cdot\vec{r}} \begin{pmatrix} 0 \\ 1 \\ a_{\downarrow\uparrow} \\ a_{\downarrow\downarrow} \end{pmatrix} + e^{-i\vec{k}'\cdot\vec{r}} \begin{pmatrix} b_{\downarrow\uparrow} \\ b_{\downarrow\downarrow} \\ 0 \\ 0 \end{pmatrix} \quad (4)$$

for spin up and down incident electrons, respectively. For an incident electron beam with spin s and incident wavevector $\vec{k} = k(\sin\theta\cos\phi, \sin\theta\sin\phi, \cos\theta)$, the tunneling conductance is

$$\sigma_{Ss}(E, \phi, \theta) = 1 + |a_{s\uparrow}|^2 + |a_{s\downarrow}|^2 - |b_{s\uparrow}|^2 - |b_{s\downarrow}|^2 \quad (5)$$

where E is the incident electron energy. For an unpolarised incident beam the total conductance is $\sigma_S = \int_0^{2\pi} d\phi \int_0^{\pi/2} \sin\theta d\theta [\sigma_{S\uparrow} + \sigma_{S\downarrow}]$. The normalised conductance is $\sigma_R = \sigma_S/\sigma_N$, where σ_N is the conductance when the superconductor is in the normal state. We obtained analytic expressions for the conductance coefficients $a_{s,s'}$ and $b_{s,s'}$, as follows:

$$a_{ji} = k_z^2 [M^{-1}]_{ij} \quad (6)$$

$$b_{ji} = -ik_z [(Zvu^{*-1} + Yuv^{*-1})M^{-1}]_{ij} - \delta_{ij} \quad (7)$$

where $Z = hH/\hbar^2$, $Y = Z + ik_z$ and

$$M_{ij} = [vu^{*-1}]_{ij} Z^2 + [uv^{*-1}]_{ij} (Z^2 + k_z^2) \quad (8)$$

and

$$u = u(\vec{k}) \ , \ v = v(-\vec{k}') \quad (9)$$

$$u^* = u^*(\vec{k}') \ , \ v^* = v^*(-\vec{k}) \quad (10)$$

u and v are 2×2 Bogoliubov transformation matrices. For a unitary gap function, these are given by[43]

$$u(\vec{k}) = \frac{[E + \epsilon(k)]\sigma_0}{[E + \epsilon(\vec{k})]^2 + \frac{1}{2}\mathrm{Tr}\Delta\Delta^\dagger(\vec{k})]^{1/2}} \quad (11)$$

$$v(\vec{k}) = \frac{-\Delta(\vec{k})}{[E + \epsilon(\vec{k})]^2 + \frac{1}{2}\mathrm{Tr}\Delta\Delta^\dagger(\vec{k})]^{1/2}} \quad (12)$$

where σ_0 is the identity matrix and $\epsilon(\vec{k}) = \sqrt{E^2 - \frac{1}{2}\mathrm{Tr}\Delta\Delta^\dagger(\vec{k})}$. For the non-unitary case, the expressions for u and v are somewhat more complicated (see Eq. (2.14) of Ref.[43]).

C. Calculations

We performed numerical calculations of the normalised conductance $\sigma_R(E)$ for the trial gap functions in Table I, for different domains and domain averaging when necessary, and for a range of the parameters Z, a, b, η_1 and η_2, resulting in more than 500 plots. We now discuss each of the gap functions in Table I in detail.

The gap function associated with the A_g order parameter is conventional (s-wave) superconductivity. Fig. 5 shows the result for an s-wave superconductor, first calculated by Blonder, Tinkham and Klapwick[35]. For small values of Z, it shows a distinctive gap edge at $E = \Delta_0 = 1$. Excess spectral area clearly increases with increasing Z, a feature that is common to all conductance curves.

The two phases for the E_g order parameter each have 8 point nodes in the $\langle 111 \rangle$ directions. Their conductance curves (not shown) feature broad peaks at energies associated with the gap maximum, but no ZBP's.

A ZBP is a feature in the conductance curves of all of the T_g phases listed in Table I. The phase $D_2(C_2) \times \mathcal{K}$ with gap function $\psi(\vec{k}) = k_x k_y$ has line nodes along $k_x = 0$ and $k_y = 0$, and there are two other equivalent domains. The conductance curves have ZBP's for the domains $\psi(\vec{k}) = k_x k_z$ and $\psi(\vec{k}) = k_y k_z$, but not for $\psi(\vec{k}) = k_x k_y$. The domain average result is shown in Fig. 6.

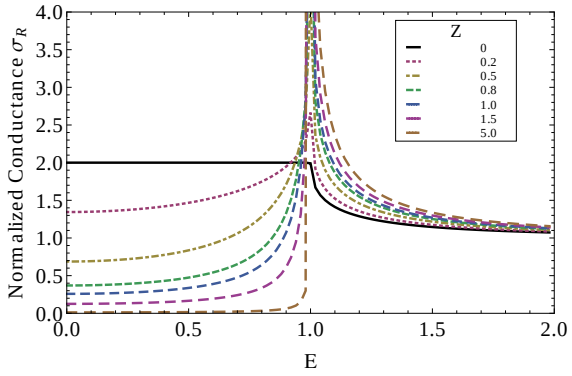

FIG. 5: (color online). Normalised conductance for a conventional superconductor (A_g).

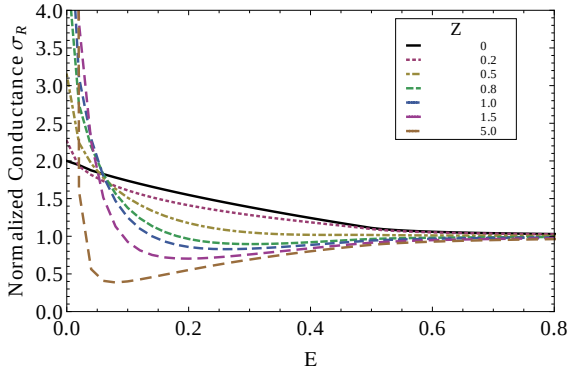

FIG. 6: (color online). Normalised conductance for the singlet phase $D_2(C_2) \times \mathcal{K}$ with gap function $\psi(\vec{k}) = k_x k_y$, averaged over three equivalent domains.

As for the remaining T_g phases, the phase $C_3 \times \mathcal{K}$ has 6 point nodes in the $\langle 001 \rangle$ directions, but these nodes disappear in the presence of an s-wave secondary OP (and the ZBP persists), as shown in Fig. 7. Note that for large Z, the ZBP evolves toward a broad, "hump-like" structure. The phase $C_3(E)$ (not shown) has 6 point nodes at $\langle 001 \rangle$ and 2 point nodes at $\langle 111 \rangle$. In the presence of a $T(D_2)$ secondary OP the $\langle 001 \rangle$ nodes disappear, and the ZBP moves away from $E = 0$. Finally, the phase $D_2(E)$ for the domain with gap function $\psi(\vec{k}) = \eta_1 k_y k_z + i\eta_2 k_z k_x$ has a line node along $k_z = 0$ and 2 point nodes at $[00 \pm 1]$. The domain average result yields a ZBP for any values of η_1 and η_2. The results for $D_2(E)$ (not shown) closely resemble those of $D_2(C_2) \times \mathcal{K}$ (shown in Fig. 6).

The triplet phase belonging to A_u is a nodeless, unitary superconductor. As shown in Fig. 8, instead of a gap edge, a sharp minimum in the conductance spectrum appears at the gap energy. This feature has been seen previously in calculations for Sr_2RuO_4[45].

The triplet phase belonging to the E_u order parameter with symmetry $T(D_2)$ is non-unitary. It has eight point nodes in the $\langle 111 \rangle$ directions on the lower branch of the gap function. The spectrum (shown in Fig. 9) has

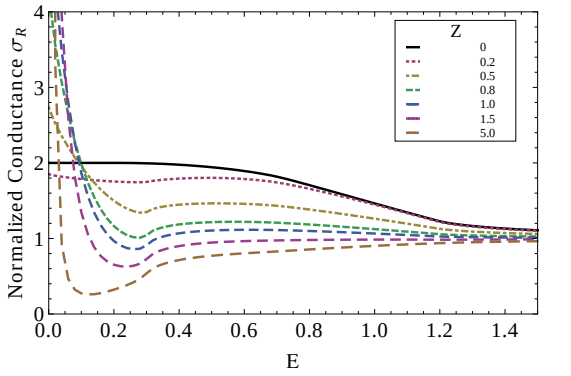

FIG. 7: (color online). Normalised conductance for the singlet phase $C_3 \times \mathcal{K}$, with gap function $\psi(\vec{k}) = k_x k_y + k_y k_z + k_x k_y + 0.2(k_x^2 + k_y^2 + k_z^2)$.

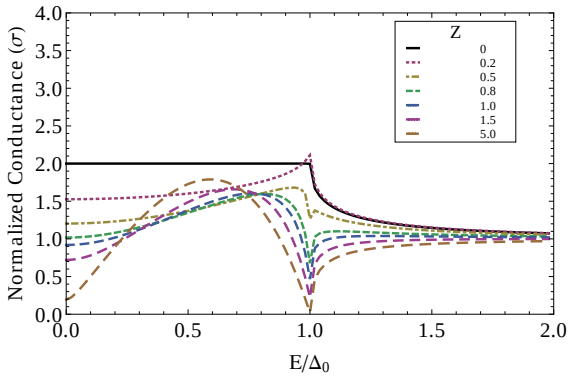

FIG. 8: (color online). Normalised conductance for the triplet phase A_u with gap function $\vec{d}(\vec{k}) = (k_x, k_y, k_z)$.

a strong peak, but not at $E = 0$. The other phase of the E_u order parameter, $D_2 \times \mathcal{K}$, is unitary, and nodeless. Its spectrum (not shown) has a peak, but not at $E = 0$.

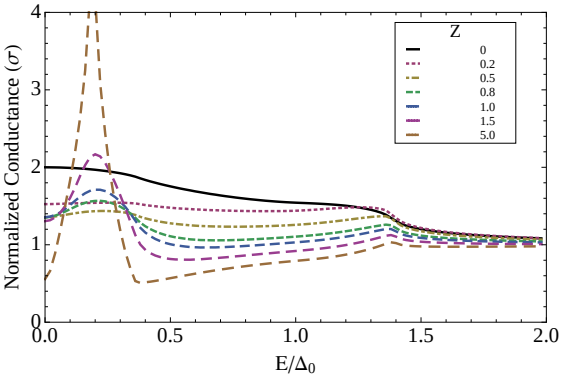

FIG. 9: (color online). Normalised conductance for the triplet phase $T(D_2)$ the gap function $\vec{d}(\vec{k}) = (k_x, \varepsilon k_y, \varepsilon k_z^2)$

The triplet phase belonging to the T_u order parameter with symmetry $D_2(C_2) \times \kappa$ has point nodes in the [001]

directions. This is a unitary case, and it does not exhibit ZBP's for $\vec{d} = (bk_y, ak_x, 0)$; however ZBP's are present for the other two domains. The domain average is shown in Fig. 10.

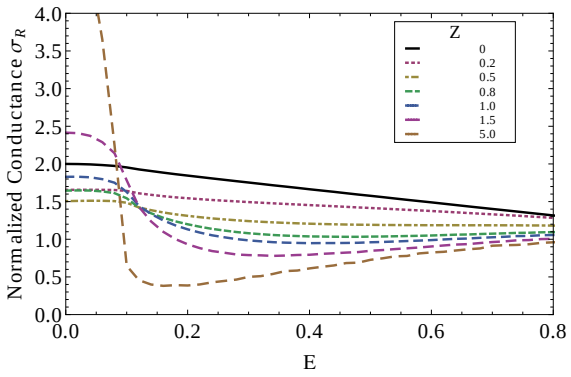

FIG. 10: (color online). Normalised conductance for the triplet phase $D_2(C_2) \times \mathcal{K}$ with gap function $\vec{d}(\vec{k}) = (bk_y, ak_x, 0)$, averaged over three equivalent domains.

As for the other triplet phases belonging to the T_u order parameter, the phase $C_3 \times \mathcal{K}$ is unitary, and nodeless, and it displays a broad peak at $E \neq 0$ (not shown). The phase $C_3(E)$ is non-unitary and has two point nodes in the $\pm$[111] directions on the lower branch of the gap function. Its spectrum (not shown) has strong peaks whose positions vary according to the choice of parameters. Finally, the phase $D_2(E)$ is non-unitary, with nodes that are not in a direction of high symmetry[46]. The domain-averaged spectra display peaks whose positions vary with the choice of parameters.

Thus, the only phase in the triplet channel that exhibits a ZBP is $D_2(C_2) \times \kappa$, which belongs to the three component OP T_u.

We conclude that there are several different pairing symmetries for a T_h crystal that can yield a conductance spectrum with a ZBP, namely $D_2(C_2) \times \mathcal{K}$, $C_3 \times \mathcal{K}$, and $D_2(E)$ (belonging to the T_g OP) in the singlet channel and $D_2(C_2) \times \mathcal{K}$ (belonging to the T_u OP) in the triplet channel. In addition, all of these candidate gap functions can account for both of the key observations of our experiment, namely the ZBP (corresponding to large Z) and the broad hump-like structure (corresponding to small Z), which implies that these features may be attributed to a single OP present on two different bands with two different values of Z.

IV. DISCUSSION

Our experimental results are apparently in disagreement with a previous measurement of scanning tunneling spectroscopy (STS) on $PrOs_4Sb_{12}$ by Suderow *et al.*[47], which observed a spectrum which closely resembles that shown in Fig. 5, *i.e.*, for an *s*-wave superconductor. However, these results can be reconciled with ours if we account for slightly different experimental conditions. First of all, we repeated the calculations within a narrow polar angle $\theta < \pi/9$ in momentum, to model the effect of a finite tunneling cone[34,48] which applies to high-impedance STS junctions in contrast to low-impedance PCS junctions. In addition, we considered different directions for the incident beam, since Ref.[47] did not identify the direction of the tunneling current with respect to the crystallographic axes. Furthermore, they reported that although their observed spectrum was reproduced in different places, it was not found over the whole surface. We found that for the tunneling current in the [011] and [111] directions and a narrow tunneling cone, the ZBP seen in Fig. 6 disappeared, and was replaced by a gap edge very similar to that in Fig. 5. Furthermore, of all the calculated spectra exhibiting ZBP's, this only occurred for the states belonging to T_g (and not the one belonging to T_u). The result of this calculation is shown in Fig. 11. Therefore, not only does this provide an explanation for

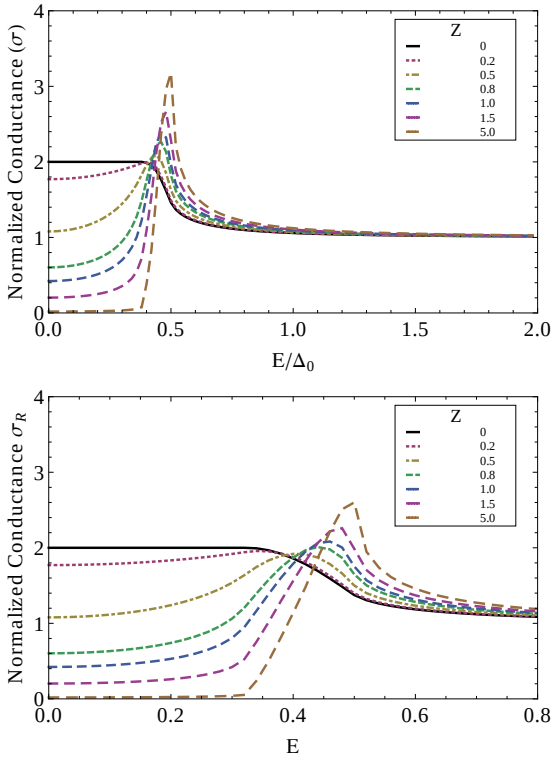

FIG. 11: (color online). Normalised conductance for the gap function $\psi(\vec{k}) = k_y k_z$ (top) and $\psi(\vec{k}) = k_x k_y + k_y k_z + k_x k_z$ for a tunneling current in the [011] direction with a narrow polar angle integration.

the difference between the results of Suderow *et al.* and ours, it also strongly suggests that the gap function has singlet pairing and belongs to the T_g order parameter.

We now discuss our results in the context of other experiments on $PrOs_4Sb_{12}$. No experiment has detected the presence of line nodes in the gap function, which

is strong evidence against the phases $D_2(C_2) \times \mathcal{K}$ and $D_2(E)$ in the singlet channel. *This leaves $C_3 \times \mathcal{K}$ in the singlet channel as the best candidate for the superconducting pairing symmetry.* Because of the secondary s-wave OP, the state is nodeless at low temperatures, in agreement with thermal conductivity measurements[16]. However, it should be noted that this proposed gap function disagrees with the μSR measurements of Aoki *et al.*[49], who concluded that superconductivity in $PrOs_4Sb_{12}$ is non-unitary. It also disagrees with the observation of broken C_3 symmetry, according to the shape of the vortex lattice[6,50].

We now offer a qualitative description of the model that we propose. Superconductivity appears on a low Z band with unconventional pairing (with symmetry $C_3 \times \mathcal{K}$) accompanied by the simultaneous appearance of a similar OP on a high Z band, along with an s-wave component. The growth of the OP on the two different bands will be governed by the same temperature dependence, but with different magnitudes. Only one T_c is required, but the growth of the s-wave component will be slower because it is a secondary OP. This may account for the evolution of the spectral features we observe, but not for the observation of two distinct T_c's. Since the OP we propose has three components, there are different scenarios that could give rise to two different T_c's. Two possibilities are: *i*) s-wave superconductivity appears first, followed by the unconventional OP that we described; or *ii*) unconventional superconductivity first, followed by a transition to an even lower symmetry superconducting state. We note that any experiment that can detect changes in symmetry below each transition would be of enormous benefit in discriminating these possibilities.

In summary, we have performed point-contact Andreev reflection spectroscopy on $PrOs_4Sb_{12}$ down to 90 mK and up to 3 T and observed evidence for unconventional superconductivity involving multiple bands. A single superconducting phase of the T_g OP, present on two bands, can account for our results. Among the possible superconducting phases of this OP, the phase $C_3 \times \mathcal{K}$ with gap function $\psi(\vec{k}) = k_x k_y + k_y k_z + k_x k_z + s$ agrees best with the results of other experiments. Our observations corroborate similar observations of multi-band superconductivity from bulk measurements, and highlight the unconventional nature of the pairing state in this heavy fermion superconductor.

Acknowledgments

Research at the University of Toronto was supported by grants from NSERC, CFI/OIT, OCE, and the Canadian Institute for Advanced Research under the Quantum Materials Program. Research at UCSD was supported by the US Department of Energy under research grant number DE FG02-04ER46105. Research at Memorial University of Newfoundland was supported by NSERC.

[1] E. D. Bauer *et al.*, Phys. Rev. B **65**, 100506(R) (2002).
[2] M. B. Maple *et al.*, J. Phys. Soc. Jpn. **71**, Sup. 23 (2002).
[3] R. Vollmer *et al.*, Phys. Rev. Lett. **90**, 057001 (2003).
[4] T. Tayama *et al.*, J. Phys. Soc. Jpn. **72**, 1516 (2003).
[5] E. E. M. Chia *et al.*, Phys. Rev. Lett. **91**, 247003 (2003).
[6] A. D. Huxley *et al.*, Phys. Rev. Lett. **93**, 187005 (2004).
[7] N. A. Frederick *et al.*, J. Low Temp. Phys. **147**, 321 (2007).
[8] N. A. Frederick, T. A. Sayles and M. B. Maple, Phys. Rev. B **71**, 064508 (2005).
[9] K. Izawa *et al.*, Phys. Rev. Lett. **90**, 117001 (2003).
[10] K. Katayama *et al.* J. Phys. SOc. Jpn. **76**, 023701 (2007).
[11] R. Joynt and L.Taillefer, Rev. Mod. Phys. **74**, 235 (2002).
[12] M. B. Maple *et al.*, J. Super. Nov. Mag **19**, 299 (2006).
[13] H. Sugawara *et al.*, Phys. Rev. B **66**, 220504 (2002).
[14] D. E. MacLaughlin *et al.*, Physica B **403**, 1132 (2008).
[15] L. Shu *et al.*, Phys. Rev. B **79**, 174511 (2009).
[16] G. Seyfarth *et al.*, Phys. Rev. Lett. **97**, 236403 (2006).
[17] R. W. Hill *et al.*, Phys. Rev. Lett. **101**, 237005 (2008).
[18] In the standard model of multiband superconductivity[19], sub-components of a single OP are expected to share a common pairing symmetry and transition temperature.
[19] H. Suhl, *et al.*, Phys. Rev. Lett. **3**, 552 (1959).
[20] G. Deutscher, Rev. Mod. Phys. **77**, 109 (2005).
[21] J. Zasadzinski, in *The Physics of Superconductors*, edited by K. H. Bennemann (Springer, New York, 2003).
[22] F. Laube, *et al.*, Phys. Rev. Lett. **84**, 1595 (2000).
[23] Z. Q. Mao *et al.*, Phys. Rev. Lett. **87**, 037003 (2001).
[24] N.L. Bobrov *et al.*, Phys. Rev. B **71**, 014512 (2005).
[25] P. Szabo *et al.*, Phys. Rev. Lett. **87**, 137005 (2001).
[26] Yu. G. Naidyuk *et al.*, J. Phys.: Cond. Mat. **10**, 8905 (1998) and references therein.
[27] G. Goll, in *Advances in Solid State Physics*, edited by B. Kramer (Springer Verlag 2005).
[28] E.D. Bauer *et al.*, J. Phys.: Cond. Mat. **13**, 4495 (2001).
[29] K. Grube *et al.*, Phys. Rev. B **73**, 104503 (2006).
[30] Using the Wexler formula, $R \cong 4\rho l/3\pi a^2 + \rho/2a$, with $\rho \approx 2$ $\mu\Omega$cm, mean free path $l \approx 350$ nm, and R the junction impedance, the contact radius, a is estimated to be ≈ 90 nm thus satisfying the ballistic criterion $a < l$.
[31] P. M. C. Rourke *et al.*, Phys. Rev. Lett. **94**, 107005 (2005).
[32] Y. Asano *et al.*, Phys. Rev. B **68**, 184506 (2003).
[33] J. Linder *et al.*, Phys. Rev. B **75**, 054518 (2007).
[34] J.Y.T. Wei, *et al.*, Phys. Rev. Lett. **81**, 2542 (1998).
[35] G.E. Blonder *et al.*, Phys. Rev. B **25**, 4515 (1982).
[36] Note that the excess area has a BCS-like temperature dependence, consistent with a fully-gapped OP; while the ZBP height deviates from such BCS-like behavior, consistent with a more complex OP having gap nodes[37].
[37] Y. DeWilde *et al.*, Phys. Rev. Lett. **72**, 2278 (1994).
[38] G. Goll *et al.*, Phys. Rev. B **52**, 6801 (1995).
[39] M.-A. Measson *et al.*, Phys. Rev. B **77**, 134517 (2008).
[40] H. Tou *et al.*, Physica B **378-380**, 209 (2006).
[41] E.E.M. Chia *et al.*, J. Phys. Cond. Mat. **17**, L303 (2005).
[42] G. E. Volovik and L. P. Gor'kov, Sov. Phys. JETP **61**, 843 (1985).
[43] M. Sigrist and K. Ueda, Rev. Mod. Phys. **639**, 239 (1991).

[44] I. A. Sergienko and S. H. Curnoe, Phys. Rev. B **70**, 144522 (2004).
[45] C. Honerkamp and M. Sigrist, J. Low Temp. Phys. **111**, 895 (1998).
[46] T. R. Abu Alrub and S. H. Curnoe, Phys. Rev. B **76**, 054514 (2007).
[47] H. Suderow, S. Viera, J. D. Strand, S. Bud'ko and P. C. Canfield, Phys. Rev. B **69**, 060504 (2004).
[48] J. Y.T. Wei, C. C. Tsuei, P. J. M. van Bentum, Q. Xiong, C. W. Chu, and M. K. Wu, Phys. Rev. B **57**, 3650 (1998).
[49] Y. Aoki, A. Tsuchiya, T. Kanayama, S. R. Saha, H. Sugawara, H. Sato, W. Higemoto, A. Koda, K. Ohishi, K. Nishiyama and R, Kadono, Phys. Rev. Lett. **91**, 067003 (2003).
[50] S. Mukherjee and D. F. Agterberg, Phys. Rev. B **74**, 174505 (2006).